A R C H I V E O F M E C H A N I C A L E N G I N E E R I N G

VOL. LXV 2018 Number 4

DOI: 10.24425/ame.2018.125442

Key words: natural convection; internal obstructions; porous enclosure; Darcy law

JAYESH SUBHASH CHORDIYA[1], *RAM VINOY SHARMA*[1]

NUMERICAL STUDY ON THE EFFECTS OF MULTIPLE INTERNAL DIATHERMAL OBSTRUCTIONS ON NATURAL CONVECTION IN A FLUID-SATURATED POROUS ENCLOSURE

The present work aims at studying the effects of orientation, size, position, and the combination of multiple internal diathermal obstructions in a fluid-saturated square porous enclosure, generally encountered in thermal insulations. The overall objective is to suppress the natural convection fluid flow and heat transfer across a differentially heated porous enclosure. To serve this purpose, multiple diathermal obstructions are employed to mechanically protrude into a porous medium. It is sought to estimate the effect of various types of orientation, clustering and alternate positioning of obstructions by considering number of obstructions (N_p), length of obstructions (λ), modified Rayleigh number (Ra^*) on local and average Nusselt number (Nu). The Darcy model for porous media is solved using Finite difference method along with Successive Accelerated Replacement scheme. One of the findings is that the value of the Nusselt number decreases by increasing both, the number of obstructions as well as the length of obstructions irrespective of its orientation and positioning. The reduction in Nusselt number is significant with obstructions attached on lower half of the hot wall and/or on upper half of cold wall. In addition, the overall reduction in Nusselt number is slightly greater with obstructions attached explicitly to the cold wall.

Nomenclature

c	specific heat, J/(kg K)
D_p	distance between obstructions
g	acceleration due to gravity, m/s^2
k	thermal conductivity, W/(m K)
K	permeability, m^2
L	length and height of enclosure, m

[1] *National Institute of Technology, Jamshedpur. Emails: jayesh.subhash@gmail.com; rvsharma.me@nitjsr.ac.in*

L_p	length of obstruction
N_p	number of obstructions
Nu	average Nusselt number
Ra^*	modified Rayleigh number
T	temperature, K
U, V	dimensionless x- and y- velocity
u, v	x- and y- velocity, m^2/s
x, y	horizontal and vertical directions, m
X, Y	dimensionless horizontal and vertical directions
α	thermal diffusivity, m^2/s
β	coefficient of thermal expansion, (/K)
θ	dimensionless temperature
μ	dynamic viscosity, Ns/m^2
ν	kinematic viscosity, m^2/s
ρ	density, kg/m^3
δ	height of obstruction
λ	dimensionless length of obstruction
ψ	dimensionless stream function
ω	acceleration factor

Subscripts

c	cold
h	hot
e	effective

1. Introduction

The use of obstacles, fins, full partitions or partial partitions in a differentially heated porous enclosure has grasped considerable attention in the recent years. The obstruction might be partial or full and placed on each or any of the sidewalls of the enclosure. Suppression of natural convection is essential if sought to decrease the rate of heat transfer in a medium, porous or not. For instance, the application of double wall spacing for building insulation, solar energy collection, etc., involve porous insulations wherein heat transfer rate is required to be very less. The literature survey reveals that there are limited studies on the effects of obstructions, especially related to their orientation, positioning, size and arrangements, on natural convection heat transfer across a porous medium.

To address the challenge of a weakly non-linear study, author of [1] examined the natural convection in a partitioned porous enclosure with a diathermal partition isolating two identical porous sublayers from one another. Similarly, in [2] natural convection in a horizontal fluid-saturated porous layer heated from bottom and sub-

divided it into a number of similar sublayers by horizontal diathermal partitions is presented. The problem of unsteady magneto-hydrodynamic natural convection in partitioned fluid-saturated porous square enclosure with internal heat generation can be found in [3]. Introducing concept of energy-streamline in field of porous medium, authors of [4] attempted to visualize natural convection in a differentially heated porous enclosure with internal flow obstructions. They indicated that using an obstruction in an enclosure is similar to reducing Darcy number of the porous medium. The average Nusselt number on the hot wall decreased compared to the no obstruction case. They also added that horizontal obstacle adds some thermal insulation effect. Not long ago, a thorough review documented in [5] emphasized the effect of a single fin position and fin length on modification of the re-circulating cells and isotherms within the porous enclosure. The rate of decrease of average Nusselt number became increasingly slower as the fin position repositioned from the bottom to top wall with the overall heat transfer rate managed by an appropriate selection of the fin position and length. Effect of diagonally positioned thin plate on natural convection flow in a porous enclosure was illustrated in [6]. Authors illustrated that heat transfer dropped with attachment of the inclined plate regardless of its position and Rayleigh number. By changing the shape of porous enclosure, other researchers also evaluated natural convection in an insulated horizontal diathermal plate inserted in a triangular porous enclosure [7]. They revealed that heat transfer reduced locally by using an insulated diathermal plate. Considering a similar model, a 2D numerical solution of natural convection in solid diathermal fin attached to porous right triangular enclosures is demonstrated in [8]. In an interesting study, authors of [9] reported a steady natural convection analysis about a heated corrugated plate implanted in a bounded porous medium. The heat transfer rate reduced, as the plate moved downward along the vertical axis of the enclosure. In a vertical porous layer separated by N equispaced partitions, the Nusselt number, in the boundary layer regime, varies inversely with $(1 + N)^{4/5}$ with the highest reduction in heat transfer attained when the partition is centrally located [10]. Back in the days, important contributions were also reported in [11], relating to the buoyancy-induced flow occurring on both sides of an impermeable vertical partition bifurcating two semi-infinite porous media at dissimilar temperatures. Authors concluded that insertion of a vertical partition in the centre of a vertical porous medium significantly reduced the net heat transfer across it.

The fundamental idea of the current study is to deviate the convection current developed within the porous enclosure because of its differential heating. Various types of orientation, size, position and combination of multiple internal diathermal obstructions are employed for this purpose to evaluate the fluid flow and heat transfer behaviour in each case. As seen from the literature, almost all are single-partition based studies. Moreover, work based on multiple diathermal partial partitions having detailed study of its orientation, size, position and combination is yet to appear in the literature. The objective of the present study is to suppress the natural convection fluid flow and heat transfer across a differentially heated

square porous enclosure with a thin, impermeable, multiple diathermal obstructions attached within it. The effect of orientation, size, position and combination of partitions is studied for the following parameters: Number of obstructions (N_p), length of obstructions (λ), modified Rayleigh number (Ra^*), orientation, clustering and alternate positioning.

2. Mathematical formulation

A fluid-saturated square porous enclosure of length and height L is differentially heated with left and right wall at temperature T_h and T_c respectively, such that $T_h > T_c$ while the top and bottom wall are insulated as shown in Fig. 1. The flow is assumed to be 2D, steady, laminar and incompressible. The porous medium is considered to be isotropic, homogenous and in local thermal equilibrium with the saturated fluid. For the current study, the distance between all the obstruction is kept at constant value of D_p which may vary from case to case. Length of each obstruction is L_p. It may be same or different for each of the obstruction depending upon the orientation and arrangement. N_p is the total number of partitions attached within the enclosure irrespective of its positioning on hot wall or cold wall. Thermophysical properties of fluid are assumed constant, except for density ρ, in momentum equation, for which Boussinesq approximation is used.

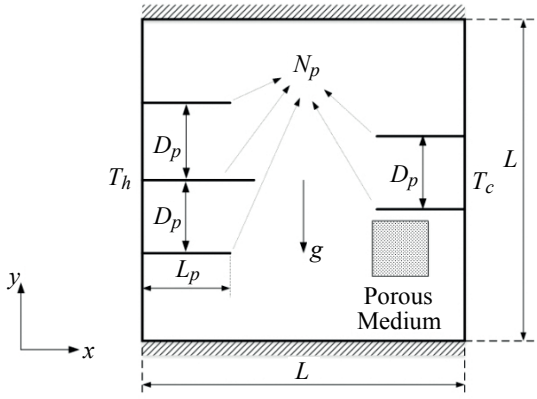

Fig. 1. Schematic diagram of a typical porous enclosure with multiple obstructions (representative purpose)

The governing equations for conservation of mass, momentum (Darcy model) and energy for porous medium in dimensional form can be written as,

$$\frac{\partial u}{\partial x} + \frac{\partial v}{\partial y} = 0, \tag{1}$$

$$u = -\frac{K}{\mu}\frac{\partial p}{\partial x}, \tag{2}$$

$$v = -\frac{K}{\mu}\left(\frac{\partial p}{\partial x} + \rho g\right), \tag{3}$$

$$\left(u\frac{\partial T_p}{\partial x} + v\frac{\partial T_p}{\partial y}\right) = \alpha_e\left(\frac{\partial^2 T_p}{\partial x^2} + \frac{\partial^2 T_p}{\partial y^2}\right). \tag{4}$$

These equations are subjected to the following boundary conditions,

$$\begin{aligned} &\textit{Left wall } (x = 0,\ 0 \leqslant y \leqslant L): && u = 0,\ \ T = T_h\,,\\ &\textit{Right wall } (x = L,\ 0 \leqslant y \leqslant L): && u = 0,\ \ T = T_c\,,\\ &\textit{Bottom} \text{ and } \textit{Top wall } (0 \leqslant x \leqslant L,\ y = 0,\ L): && v = 0,\ \ \partial T/\partial y = 0\,. \end{aligned} \tag{5}$$

A typical matching condition at the obstruction is given as,

$$\begin{aligned} &\textit{Obstruction attached to hot wall } (0 \leqslant x \leqslant L_p;\ y = H_p):\\ &\qquad v = 0,\ \ \partial T/\partial y^- = \partial T/\partial y^+,\\ &\textit{Obstruction attached to cold wall, } (L - L_p \leqslant x \leqslant L;\ y = H_p):\\ &\qquad v = 0,\ \ \partial T/\partial y^- = \partial T/\partial y^+. \end{aligned} \tag{6}$$

Following dimensionless variables are used to simplify the above equations and boundary conditions,

$$X = \frac{x}{L};\quad Y = \frac{y}{L};\quad U = \frac{u}{\alpha_e/L};\quad V = \frac{v}{\alpha_e/L};\quad \theta = \frac{T - T_c}{T_h - T_c}\,. \tag{7}$$

Following dimensionless parameters are used while non-dimensionalizing the above equations and boundary conditions,

$$\mathrm{Ra}^* = \frac{Kg\beta\Delta TH}{\nu\alpha_e};\quad \lambda = \frac{L_p}{L};\quad \delta = \frac{H_p}{L}\,. \tag{8}$$

Velocities are represented in terms of stream function (ψ). The relation is given as,

$$U = \frac{\partial\psi}{\partial Y};\quad V = -\frac{\partial\psi}{\partial X}\,. \tag{9}$$

Using the above relations along with dimensionless variables and parameters, Eq. (1)–(6) can be rewritten in non-dimensional stream function and vorticity formulation as,

$$\frac{\partial^2\psi}{\partial X^2} + \frac{\partial^2\psi}{\partial Y^2} = -\mathrm{Ra}^*\frac{\partial\theta}{\partial X}, \tag{10}$$

$$\frac{\partial\psi}{\partial Y}\frac{\partial\theta}{\partial X} - \frac{\partial\psi}{\partial X}\frac{\partial\theta}{\partial Y} = \frac{\partial^2\theta}{\partial X^2} + \frac{\partial^2\theta}{\partial Y^2}, \tag{11}$$

with boundary conditions,

$$\begin{aligned} &\textit{Left wall } (X = 0,\ 0 \leqslant Y \leqslant 1): && \psi = 0,\ \ \theta = 1, \\ &\textit{Right wall } (X = 1,\ 0 \leqslant Y \leqslant 1): && \psi = 0,\ \ \theta = 0, \\ &\textit{Bottom} \text{ and } \textit{Top wall } (0 \leqslant \mathrm{X} \leqslant 1,\ \mathrm{Y} = 0, 1): && \psi = 0,\ \ \partial\theta/\partial Y = 0\,. \end{aligned} \tag{12}$$

Appropriate matching condition at the obstruction becomes,

$$\begin{aligned} &\textit{Obstruction attached to hot wall } (0 \leqslant X \leqslant \lambda;\ Y = \delta): \\ &\qquad \psi = 0,\ \ \partial\theta/\partial Y^{-} = \partial\theta/\partial Y^{+}, \\ &\textit{Obstruction attached to cold wall } (1 - \lambda \leqslant X \leqslant 1;\ Y = \delta): \\ &\qquad \psi = 0,\ \ \partial\theta/\partial Y^{-} = \partial\theta/\partial Y^{+}. \end{aligned} \tag{13}$$

The above equations are numerically solved and the results are analysed qualitatively as well as quantitatively. Qualitative outcomes are manifested using streamlines and isotherms. On the other hand, quantitative outcome is evaluated by calculating the Nusselt number, local ($\mathrm{Nu}_{h,c}$) as well as average (Nu).

$$\mathrm{Nu}_{h,c} = -\left.\frac{\partial\theta}{\partial X}\right|_{X=0,1}, \tag{14}$$

$$\mathrm{Nu} = \int_0^1 \mathrm{Nu}_{h,c}(Y)\,\mathrm{d}Y. \tag{15}$$

3. Numerical procedure

The coupled partial differential governing equations are converted into algebraic equations using Finite Difference Method (FDM) and solved by Successive Accelerated Replacement (SAR) scheme. Central differencing with second-order accuracy is used to discretise governing equations, while second-order forward and backward differencing is employed at the wall boundaries. The stream function and temperature have been solved using SAR scheme for all inner grid points. A suitable value of accelerating factor (ω) is chosen based on the accuracy obtained with regards to number of iterations required to attain convergence. Local Nusselt number along hot and cold wall are estimated and average Nusselt number is calculated by numerically integrating them using Simpson's 1/3$^{\mathrm{rd}}$ rule.

3.1. SAR scheme

In a problem of spherical porous medium [12, 13] and a three-dimensional porous medium [14], have illustrated the applicability of the SAR scheme for solving system of partial differential equations in the study of two-dimensional

natural convection fluid flow and heat transfer in porous media. The basic idea of this scheme is to guess the profile for each transport property that satisfies the boundary conditions. If ξ is a transport property and the error in a typical governing equation at a grid point (i, j) at n^{th} iteration is $\tilde{\xi}^n_{ij}$. Then, $(n+1)^{\text{th}}$ approximation of the variable ξ is obtained as,

$$\xi^{n+1}_{ij} = \xi^n_{ij} - \omega \frac{\tilde{\xi}^n_{ij}}{\partial \tilde{\xi}^n_{ij} \big/ \partial \xi^n_{ij}} \,. \tag{16}$$

The accelerating factor, ω, varies from 0 to 2. The criterion set for convergence of stream function at all inner grid points is described as below. Value of ε is the error tolerance limit with a small positive value.

$$\frac{\sum_{i=2}^{i_{\max}-1} \sum_{j=2}^{j_{\max}-1} \left| \xi^{n+1}_{ij} - \xi^n_{ij} \right|}{\sum_{i=2}^{i_{\max}-1} \sum_{j=2}^{j_{\max}-1} \left| \xi^{n+1}_{ij} \right|} < \varepsilon. \tag{17}$$

The important feature of this method is that the corrected value of the variable is immediately used upon becoming available. A numerical code based on this method is developed to solve the governing equations along with prescribed boundary conditions.

4. Results and discussion

The discretized equations and boundary conditions are numerically solved to evaluate the effect of orientation, size, position and combination of multiple internal diathermal obstructions on the natural convection heat transfer and fluid flow. A non-dimensional numerical analysis is performed for following parameters: number of obstructions (N_p), length of obstructions (λ), modified Rayleigh number (Ra^*), orientation, clustering and alternate positioning. An in-house computational code is written to solve the current numerical problem. Grid sensitivity test was conducted for $\text{Ra}^* = 10 \div 1000$ for mesh size of 40×40 to 100×100. Based on the number of iterations required and accuracy of average Nusselt number, it was found that grid size of 80×80 yields satisfactory results and hence it was used for all cases. The value of acceleration factor has been chosen as 1.5 for $\text{Ra}^* \leqslant 250$ and 0.5 for $\text{Ra}^* > 250$ to maintain a stable solution. Obstructions attached on the wall are equispaced, i.e., not only the distance between the obstructions is same but also the distance between the obstruction and top as well as bottom wall is also same. All precautions are taken to make sure that obstructions pass through the grid points. However, an exception occurs for $N_p = 2$, 5 and 8. In such cases, there

is division of L by 3 or multiple of 3 which yields an irrational value of δ. The solution for such singularity is that the mesh size should be a multiple of 3 as well. Hence, for such cases where, $N_p = 2$, 5 and 8, a mesh size of 90×90 is chosen.

4.1. Code validation

Pertaining to the present configuration, the present code has been subjected to two validation checks. The code is verified by comparing it with, first, a classical problem of natural convection in differentially heated square porous enclosure without any obstruction or partition; second, square porous enclosure with straight horizontal obstruction having varying length.

4.1.1. Validation of code for porous enclosure without obstruction

Firstly, the code is compared against the benchmark solutions of a classical natural convection problem in a differentially-heated square porous cavity. Here, the left wall is hot, right wall is cold and top and bottom walls are insulated. Darcy's model has been used to describe the flow in porous medium. Table 1 shows the comparison of average Nusselt number values of previously reported results with present result.

Table 1.
Comparison of average Nusselt number for porous enclosure without obstruction with previously reported results

Authors	Ra^*		
	10	**100**	**1000**
Walker and Homsey [15]		3.097	12.96
Bejan [16]		4.200	15.8
Beckerman et al. [17]		3.113	
Gross et al. [18]		3.141	13.448
Manole and Lage [19]		3.118	13.637
Moya et al. [20]	1.065	2.801	
Baytas and Pop [21]	1.079	3.160	14.060
Travisan and Bejan [22]	1.080	3.270	18.380
Present Study	1.071	3.284	16.127

4.1.2. Validation of code for porous enclosure with horizontal diathermal obstruction

Secondly, the code is authenticated against the work [11] which is related to natural convection in porous enclosure with internal obstructions. Contrary to the previous problem, here the left wall is cold and the right wall is hot. It consists of

an internal diathermal obstruction attached on cold wall. The length of obstruction λ varies from 0 to 1 with position being fixed at $\delta = 0.5$ from bottom. Table 2 shows the comparison of present numerical work for $Ra^* = 50$ and 100.

Table 2.
Comparison of average Nusselt number for porous enclosure with horizontal obstruction/partition with results reported by Bejan [11]

	$Ra^* = 50$		$Ra^* = 100$	
λ	Bejan [11]	Present study	Bejan [11]	Present study
0	1.897	1.912	3.433	3.284
0.25	1.721	1.663	2.855	2.726
0.5	1.423	1.410	2.273	2.245
0.75	1.286	1.282	1.914	1.917
1	1.275	1.272	1.876	1.873

The numerical comparison between the results obtained from the present computational code agrees well in accordance with the results presented in literature. Thus, the code can be endorsed to study the problem stated in the current paper with greater assurance.

4.2. Effect of number of obstructions

The suppression of natural convection within the porous enclosure brought by introduction of multiple obstructions can be well studied by comparing it with the case of no obstruction as well as one full obstruction. The overall objective is to deviate the fluid flow within the enclosure in order to fully utilize the available space, since the convection current is bound to flow in either clockwise or anti-clockwise direction. Fig. 2 illustrates the streamlines and isotherms developed within a differentially square porous enclosure with and without obstructions.

It may not be always feasible to employ a full partition across a porous insulation. Thus, introducing multiple number of obstructions seems to be a reasonable approach. Fig. 3 illustrates the fluid flow behaviour for multiple obstructions attached on hot and cold wall with length fixed at 0.4 and for $Ra^* = 1000$. Firstly, it can be observed that in both the cases (Fig. 3a and Fig. 3b), the value of Nu decreases with increasing number of obstructions. This is because as the number of obstructions increases, the degree of deviation increases for both streamlines and isotherms. The magnitude of maximum absolute stream function also keeps on dropping. The inner stagnant partition of stream function can be seen to decreases in size as number of obstructions are increased. Also, the isotherms are seen to abruptly change its path across any of the obstructions observed separately. This may be attributed to the flow of convection current. In this case, the flow is in clockwise direction, as indicated by the negative values of stream functions. This means that, in the immediate upper part of obstruction, there is the flow of cold fluid

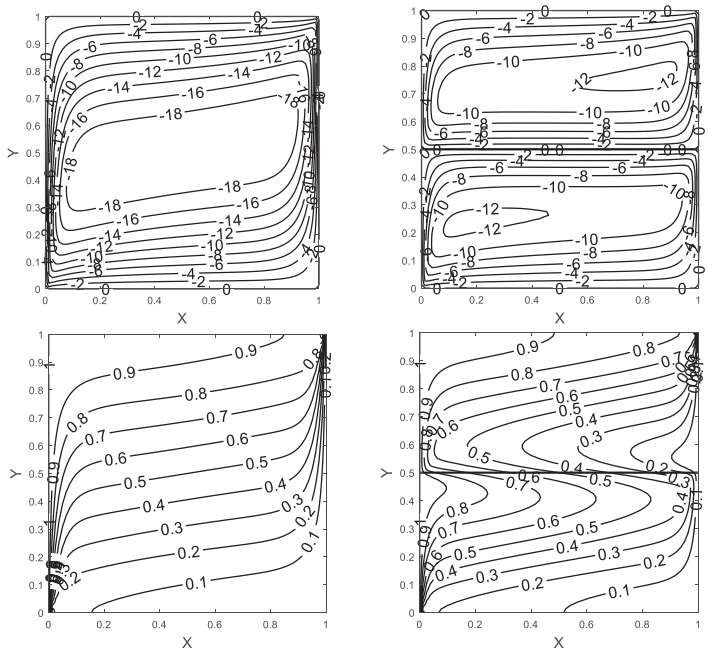

(a) $|\psi|_{\max} = 19.81$; Nu = 16.13 (b) $|\psi|_{\max} = 12.37$; Nu = 12.85

Fig. 2. Streamlines (up) and isotherms (down) in a porous enclosure with (a) no obstruction; (b) one full obstruction at $\delta = 0.5$ ($\mathrm{Ra}^* = 1000$)

while in the immediate lower part of obstruction there is the flow of hot fluid. This creates a significant temperature difference across the obstruction and hence there is the sudden deviation in its path. Consequently, more the number of obstructions, more will be the deviations. In addition, the drop in Nu values is significantly high as compared to the case depicted in Fig. 1.

Further, Fig. 4 shows the variation of average Nusselt number for various values of N_p, plotted for $\mathrm{Ra}^* = 1000$ and $\lambda = 0.25$, 0.5 and 0.75. The value of Nu continuously drops with increasing number obstructions irrespective of the value of λ. However, it can be seen that the relation of Nu with N_p is largely linear for lower value of λ. This relation becomes increasingly quadratic as the value of N_p approaches 0.5 and further. It can be noticed that, the drop in Nu values is substantial for $N_p \leqslant 5$. For values of $N_p > 5$, the drop in Nu values is not very significant. Another noticeable fact is that irrespective of the values of λ and N_p, the value of Nu for obstructions attached to cold wall is always lower than the values of Nu for obstructions attached to hot wall. This may be attributed to the fact that the downward flow of fluid near the cold side wall is already very delayed (even when no obstructions are employed). Introducing obstructions on cold wall further delays the flow causing slower movement of fluid from cold wall to hot wall and hence lowers the rate of heat transfer and consequently lowers Nusselt number.

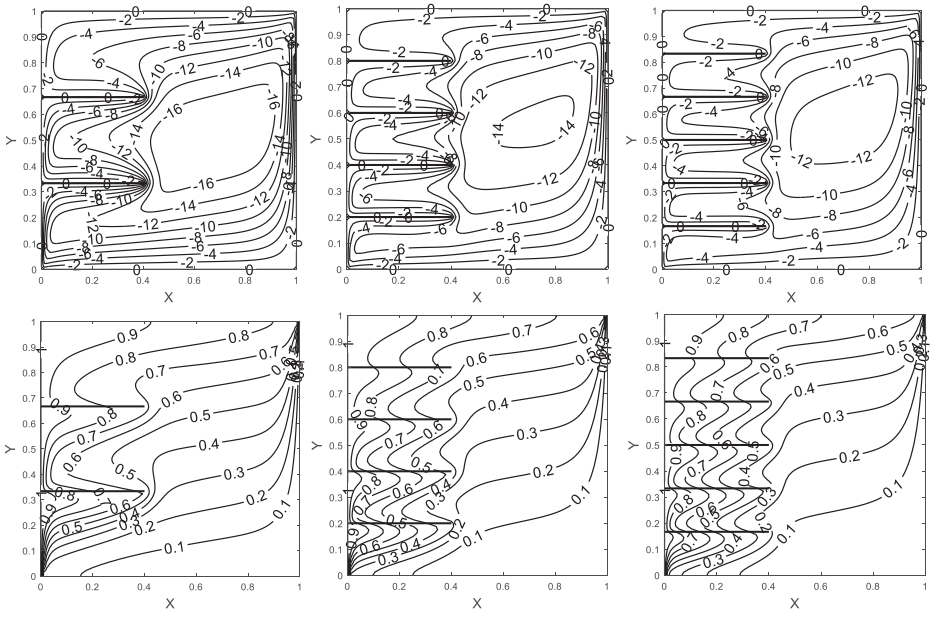

$|\psi|_{\max} = 17.64$; Nu = 12.49 $|\psi|_{\max} = 14.64$; Nu = 8.66 $|\psi|_{\max} = 13.03$; Nu = 7.01

(a) Multiple obstructions attached on hot wall ($N_p = 2$, 4 and 5)

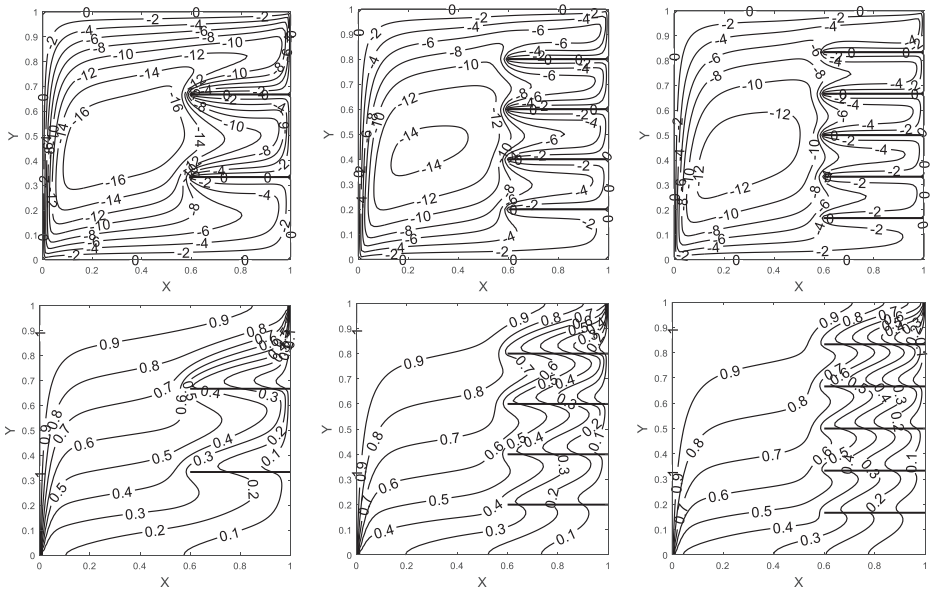

$|\psi_{\max} = 17.63$; Nu = 11.58 $|\psi|_{\max} = 14.35$; Nu = 7.87 $|\psi_{\max} = 13.03$; Nu = 6.67

(b) Multiple obstructions attached on cold wall ($N_p = 2$, 4 and 5)

Fig. 3. Streamlines (up) and isotherms (down) in a porous enclosure having multiple number of equispaced obstructions attached to: (a) hot wall, (b) cold wall ($\mathrm{Ra}^* = 1000$, $\lambda = 0.4$

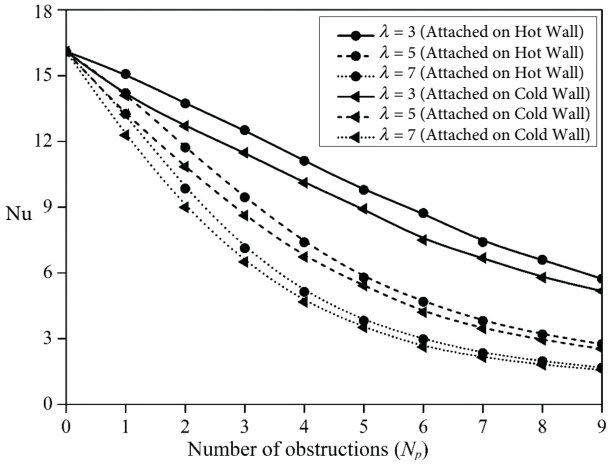

Fig. 4. Variation of average Nusselt number with number of obstructions for different lengths of obstruction ($Ra^* = 1000$; $\lambda = 0.25$, 0.5 and 0.75)

4.3. Effect of length of obstructions

Similarly, as the number of obstructions affect the fluid flow, its length also play a vital role in deviating the natural convection flow. Fig. 5 illustrates the streamlines and isotherms developed within the porous enclosure having varying length of obstructions attached on hot and cold wall for $Ra^* = 1000$ and $N_p = 4$. Similar to the effect of number of obstructions, the effect of increasing the length of obstruction is to decrease the value of Nu and $|\psi|_{\max}$. However, here, the value of $|\psi|_{\max}$ can be seen to drop to a much smaller value as the space for free movement of fluid has been cut short by large amount as the value of λ increases. In addition, the values for obstructions attached to cold wall are smaller than those for obstructions attached to hot wall, which was also seen in the previous case.

Fig. 6 illustrates the variation of average Nusselt number for various values of λ, plotted for $Ra^* = 1000$ and $N_p = 3$, 5 and 7. The value of Nu constantly drops with increasing the length of obstructions irrespective of the value of N_p. Similarly to the previous case, it can be seen that the relation of Nu with λ is typically linear for lower value of N_p. This relation becomes gradually quadratic as the value of N_p approaches to 5 and further. It can be noticed that, the drop in Nu values is substantial for $\lambda \leqslant 0.5$. For values of $\lambda > 0.5$, the drop in Nu values is not very significant. Again, irrespective of the values of λ and N_p, the value of Nu for obstructions attached to cold wall is always lower than the values of Nu for obstructions attached to hot wall for the same reason mentioned earlier. In order to understand the local effect of obstructions on fluid flow along the respective walls, it is imperative to analyse the variation of local Nusselt number along hot and cold wall, as shown in Fig. 7 which is plotted for $Ra^* = 1000$; $\lambda = 0.3$; $N_p = 2$ and 5. It can be clearly seen from the figure that, there is a noticeable rise

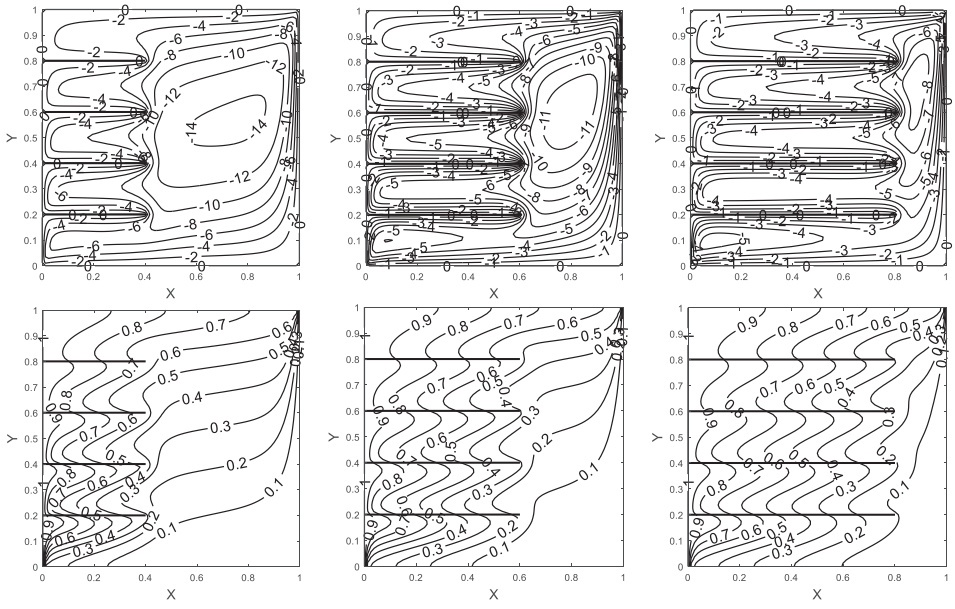

$|\psi|_{\max}$ = 14.35; Nu = 8.66 $|\psi|_{\max}$ = 11.69; Nu = 6.36 $|\psi|_{\max}$ = 8.67; Nu = 4.77

(a) Equispaced obstructions with varying length attached on hot wall (λ = 0.4, 0.6 and 0.8)

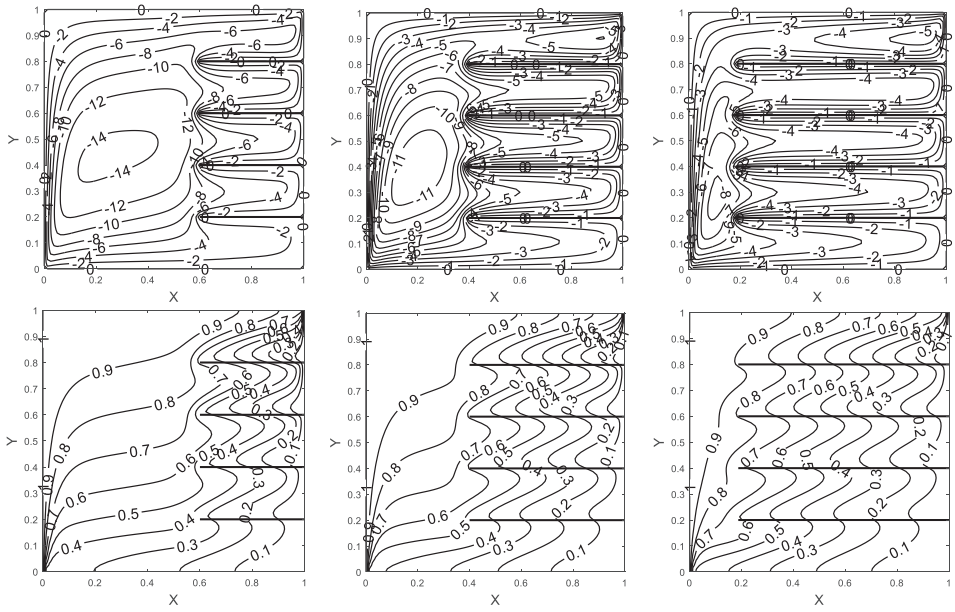

$|\psi|_{\max}$ = 14.35; Nu = 7.87 $|\psi|_{\max}$ = 11.69; Nu = 5.78 $|\psi|_{\max}$ = 8.42; Nu = 4.27

(b) Equispaced obstructions with varying length attached on cold wall (λ = 0.4, 0.6 and 0.8)

Fig. 5. Streamlines (up) and isotherms (down) in a porous enclosure having four equispaced obstructions with varying length attached to: (a) hot wall, (b) cold wall ($Ra^* = 1000$, $N_p = 4$)

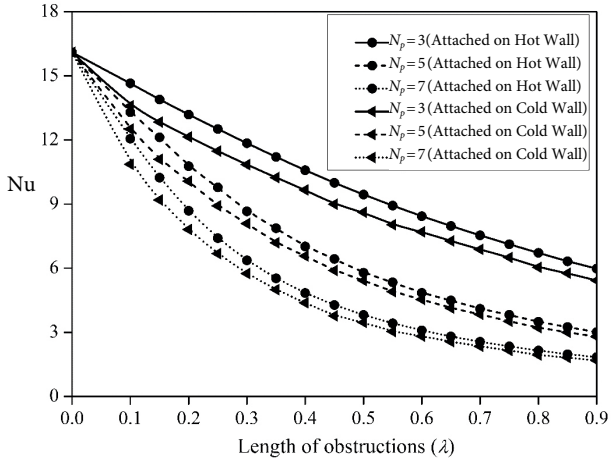

Fig. 6. Variation of average Nusselt number with length of obstructions for different number of obstructions ($Ra^* = 1000$; $N_p = 3$, 5 and 7)

in the curve at the enclosure right where obstruction is attached. For obstructions attached on hot wall, this abrupt rise in the value of local Nusselt number which decreases with increase in enclosure height. This may be because the lower half of hot wall encounters the cold fluid present in the bottom of enclosure. Hence, there is higher temperature difference in the lower half of hot wall and consequently higher temperature gradient. This fluid heats up, and rises upwards causing a decrease in the temperature difference between hot wall and fluid as it rises. Hence, it can be seen in Fig. 7a that the abrupt rise in local Nu on hot wall decreases with increase in height of the enclosure. Similar reasoning applies to upper half of cold wall where hot fluid from top part of enclosure encounters upper half of cold wall creating higher temperature gradient. The fluid cools down and moves downwards which decreases the temperature difference between cold wall and fluid

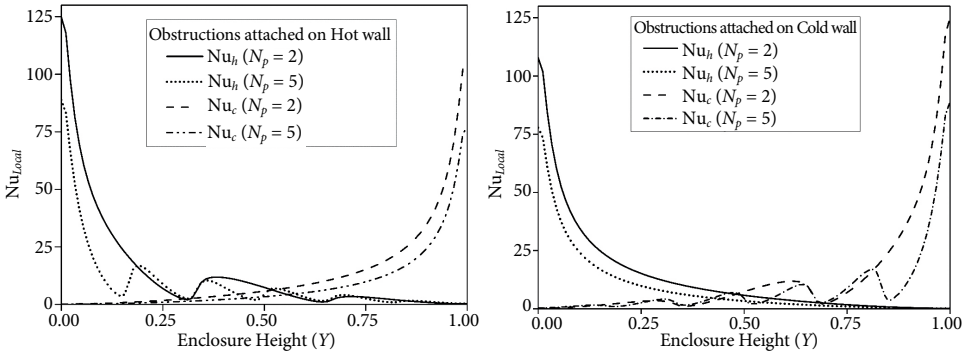

(a) Obstructions attached on hot wall (b) Obstructions attached on cold wall

Fig. 7. Variation of local Nusselt number with enclosure height (Ra^*=1000; λ=0.3; N_p=2 and 5)

as it increasingly becomes cooler and cooler. This behaviour of local Nu can be reflected in Fig. 7b where abrupt rise in local Nu increases as height of enclosure increases.

4.4. Effect of various types of orientations of obstructions

In the analysis so far, the length of all the obstructions involved in an enclosure have been maintained constant. The effect of orientating the obstructions differently, i.e., changing the length of all the partitions to form a specific orientation for the deviation of fluid flow has been discussed in this section. Thereby, six different types of orientations attached on hot wall and cold wall respectively that are considered in this study are:

1) concave orientation (type: H-1 and C-1),
2) convex orientation (type: H-2 and C-2),
3) ascending steps orientation (type: H-3 and C-3),
4) descending steps orientation (type: H-4 and C-4),
5) alternate small-big orientation (type: H-5 and C-5),
6) alternate big-small orientation (type: H-6 and C-6).

The effect of orientations has been analysed for above mentioned cases and depicted in Fig. 8 and Fig. 9. The value of N_p is fixed to 5 in order to maintain the symmetricity of the orientation. The value of λ for each obstruction of every case is given in Table 3. The effect of increasing the length and number of obstructions in each orientation is predicted to follow the similar trend as discussed in above sections. In Table 3, the obstructions are ranked from top to bottom, i.e., the length of topmost partition is denoted as λ_1 and the length of obstruction nearest to bottom wall is denoted by λ_5 and so on.

Table 3.
Values of length of obstructions (λ) considered for various types of orientations under study

Type of orientation	λ_1	λ_2	λ_3	λ_4	λ_5
Typ1 H-1 / C-1	0.125	0.25	0.5	0.25	0.125
Typ1 H-2 / C-2	0.5	0.25	0.125	0.25	0.5
Typ1 H-3 / C-3	0.1	0.2	0.3	0.4	0.5
Typ1 H-4 / C-4	0.5	0.4	0.3	0.2	0.1
Typ1 H-5 / C-5	0.25	0.5	0.25	0.5	0.25
Typ1 H-6 / C-6	0.5	0.25	0.5	0.25	0.5

A general glance at the contours reveal that whenever an obstruction of larger length is present in the lower half of hot wall and upper half of cold wall (which are the areas of high temperature gradients, as discussed earlier), the drop in the values of $|\psi|_{\max}$ and Nu is slightly greater. For instance, comparing the concave and convex type of orientations i.e., Figs. 8a, 8b, 9a and 9b, we clearly see that in concave type of orientation (Figs. 8b and 9b) there is a longer length of obstruction

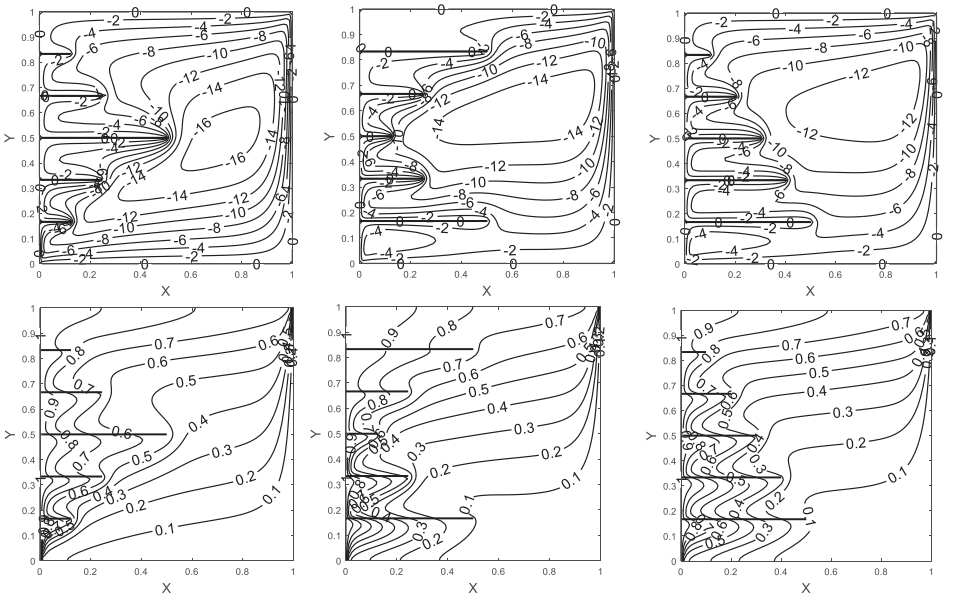

$|\psi|_{max}$ = 16.73; Nu = 10.54
(a) Type H-1

$|\psi|_{max}$ =15.30; Nu =9.45
(b) Type H-2

$|\psi|_{max}$ = 13.31; Nu = 8.64
(c) Type H-3

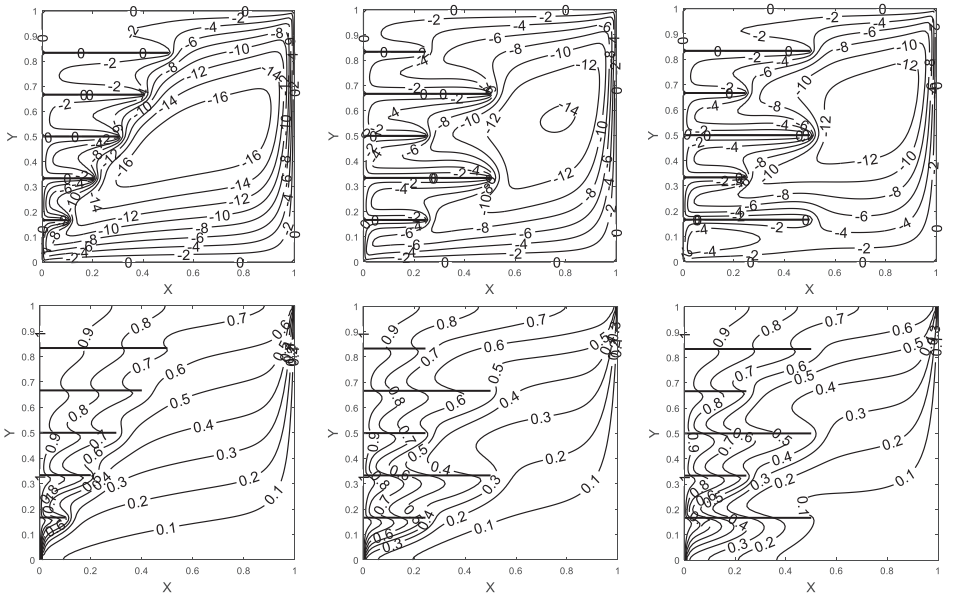

$|\psi|_{max}$ = 17.54; Nu = 10.57
(d) Type H-4

$|\psi|_{max}$ = 14.12; Nu = 8.3
(e) Type H-5

$|\psi|_{max}$ = 13.67; Nu = 7.77
(f) Type H-6

Fig. 8. Streamlines (up) and isotherms (down) in a porous enclosure having equispaced obstructions with structured-orientations attached to hot wall ($Ra^* = 1000$, $N_p = 5$)

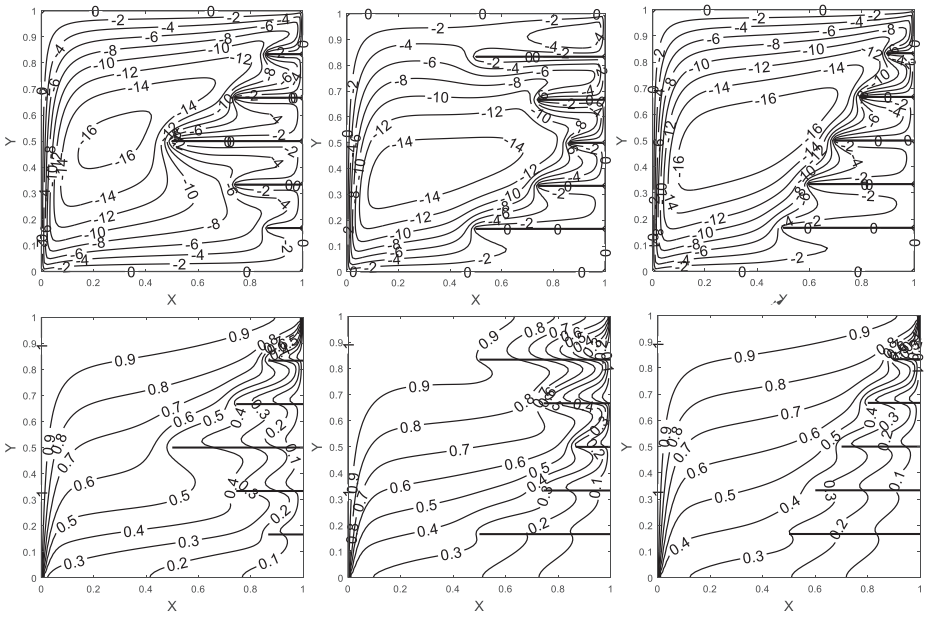

$|\psi|_{\max}$ = 16.54; Nu = 9.61
(a) Type C-1

$|\psi|_{\max}$ = 15.15; Nu = 8.77
(b) Type C-2

$|\psi|_{\max}$ = 17.54; Nu = 9.83
(c) Type C-3

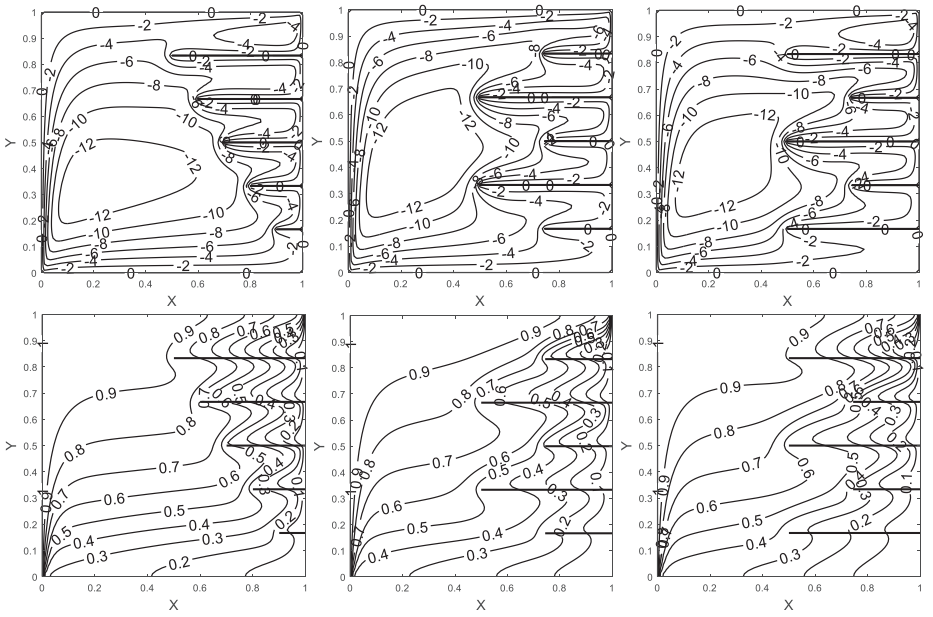

$|\psi|_{\max}$ = 13.31; Nu = 8.20
(d) Type C-4

$|\psi|_{\max}$ = 13.99; Nu = 7.6
(e) Type C-5

$|\psi|_{\max}$ = 13.56; Nu = 7.21
(f) Type C-6

Fig. 9. Streamlines (up) and isotherms (down) in a porous enclosure having equispaced obstructions with structured-orientations attached to cold wall ($Ra^* = 1000$, $N_p = 5$)

in the lower half of hot wall and upper half of cold wall, respectively; while in the case of convex type of orientation (Figs. 8a and 9a), a longer length of obstruction is present in the central portion only. Consequently, the value of $|\psi|_{\max}$ and Nu are lower for concave type than that for convex type. Going by this ideology, it can be easily manifested that Nu value for type H-3 < type H-4 while that for type C-3 > type C-4. The highest drop in Nusselt number is obtained for type H-6 and C-6 wherein, there is a greater number of longer obstructions than shorter ones.

An overall effect of such orientations can be estimated by observing the variation in the values of average Nusselt number for a wide range of modified Rayleigh number. Such a variation is demonstrated in Fig. 10.

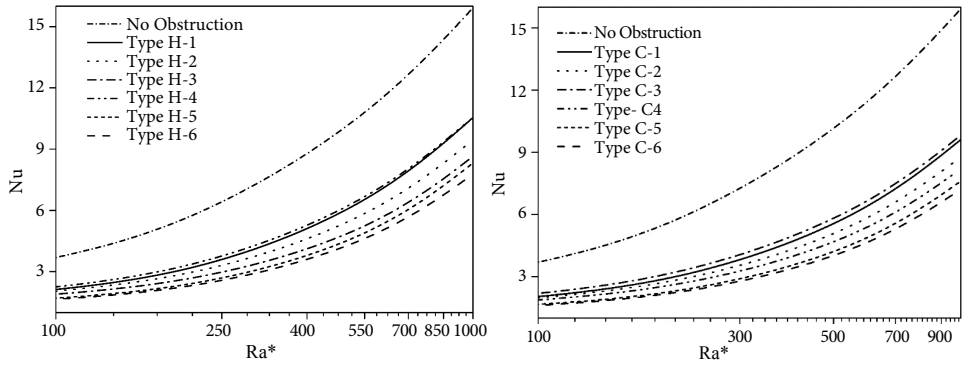

(a) Obstructions oriented on hot wall (b) Obstructions oriented on cold wall

Fig. 10. Variation of average Nusselt number with modified Rayleigh number for various types of orientations of obstructions

It can be clearly noticed from the figure that, irrespective of the type of orientation, the values of Nusselt number always increase with an increase in the values of Ra^*. This is because, as, Ra^* increases, the buoyancy strength of fluid increases, this makes the movement of fluid within the enclosure comparatively easier and quicker. Another fact that is clearly noticeable is that, as compared to the Nu value of porous enclosure with no obstruction, the Nu value of enclosure having any type of orientation is substantially lower. The average percentage reduction in Nu for lower values of Ra^* is about 65% while the average reduction in Nu values for higher values of Ra^* is about 71%. Hence, the effect of orientation is more pronounced for higher values of Ra^*. The order of orientation having decreasing values of Nu is as follows:

- For obstructions attached on hot wall:
  Type H-4 > Type H-1 > Type H-2 > Type H-3 > Type H-5 > Type H-6;
- For obstructions attached on cold wall:
  Type C-3 > Type C-1 > Type C-2 > Type C-4 > Type C-5 > Type C-6.

4.5. Effect of clustering of obstructions

Obstructions can be arranged within a porous enclosure in numerous types of ways with the view of obstructing the fluid flow. One way is to group few numbers of obstructions in a cluster and position it in different location. In the current study, three types of clustering has been taken into consideration, namely,

1. Bottom clustering,
2. Middle clustering,
3. Top clustering.

These clustered partitions are attached on both hot and cold wall separately with same length of every obstruction in a cluster. Fig. 11 demonstrates streamlines and isotherms for aforementioned three types of clustering with $N_p = 4$ and $\mathrm{Ra}^* = 1000$. As seen from Fig. 11, there is considerable decrease in the values of Nu and $|\psi|_{\max}$ as compared to those of porous enclosure without any obstructions. It can be noticed that, when the cluster is present on the lower half of hot wall or in the upper half of cold wall, the reduction in Nu values is considerably larger, i.e., the bottom clustering in Fig. 11a and top clustering in Fig. 11b has the lowest value of Nu in their corresponding figures. This is because the presence of clustered obstructions mechanically isolates the major space in these high temperature gradient regimes thus making it difficult for the fluid to initiate or continue its movement in the convection current cycle. Now, because these convective-dominant areas are partially blocked for fluid movement, the strength of flow also decreases, which can be depicted from $|\psi|_{\max}$ values. The decreasing order of the values of $|\psi|_{\max}$ is:

- for obstructions attached to hot wall:
  Top clustering > Middle clustering > Bottom clustering,
- for obstructions attached to cold wall:
  Bottom clustering > Middle clustering > Top clustering.

Similar is the decreasing order of the values of Nu. In addition, as compared to the Nu value for porous enclosure without any obstruction, the reduction in porous enclosure with bottom-clustered obstructions attached on hot wall is about 23% while that for top-clustered obstructions attached on cold wall is about 25%. Here again, the reduction in Nu is more for obstructions attached on cold wall than those attached on hot wall.

Fig. 12 illustrates the variation of average Nusselt number with respect to number of obstructions in a cluster for $\lambda = 0.25$ and 0.75. As seen from the graph, the value of Nu continuously decreases with increasing values of N_p irrespective of the values of λ. For clustered obstructions attached on hot wall, top clustering do not show any considerable decrease in the values of Nu. Similarly, for clustered obstructions attached on cold wall, bottom clustering do not display any significant drop in the values of Nu. Maximum reduction is obtained for Middle clustering having longer length of obstruction irrespective of whether clustering is on hot wall or cold wall. In addition, it can be noticed that, for $N_p \geqslant 3$, the drop in Nu is very negligible irrespective of the type of clustering, size or position.

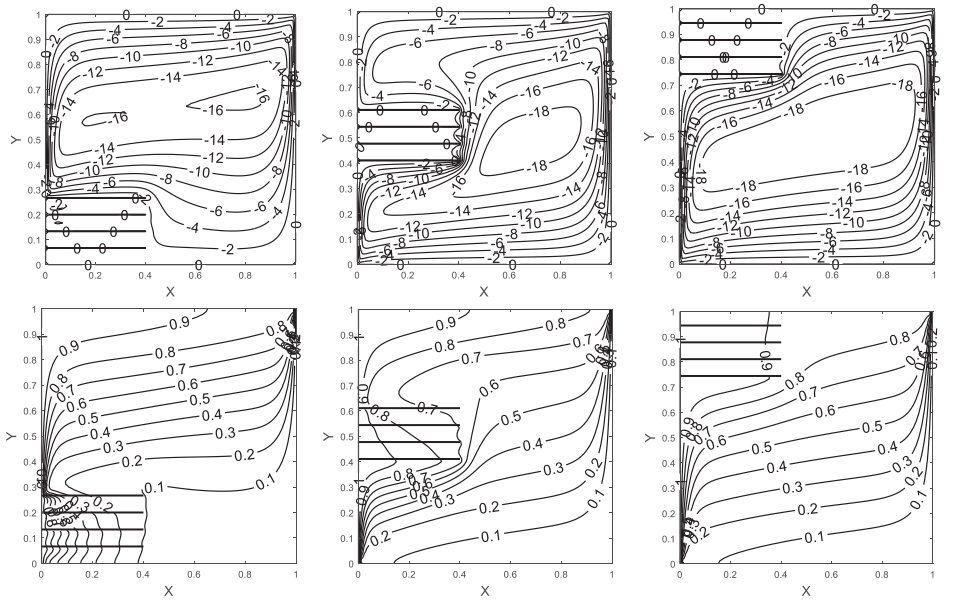

$|\psi|_{max}$ = 16.202; Nu = 12.31 $|\psi|_{max}$ = 18.99; Nu = 12.97 $|\psi|_{max}$ = 19.98; Nu = 15.04

(a) Clustered obstructions attached on hot wall (*Bottom, Mid* and *Top clustering*)

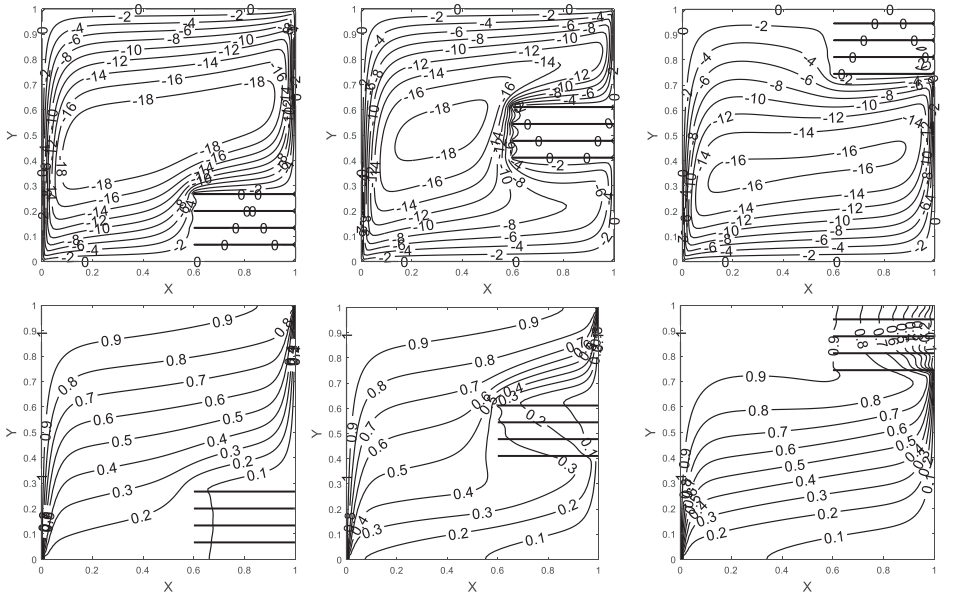

$|\psi|_{max}$ = 19.98; Nu = 14.07 $|\psi|_{max}$ = 18.74; Nu = 12.35 $|\psi|_{max}$ = 16.37; Nu = 12.14

(b) Clustered obstructions attached on cold wall (*Bottom, Mid* and *Top clustering*)

Fig. 11. Streamlines (up) and isotherms (down) in a porous enclosure having equispaced and clustered obstructions attached to: (a) hot wall, (b) cold wall. ($Ra^* = 1000$, $N_p = 4$, $\lambda = 0.4$)

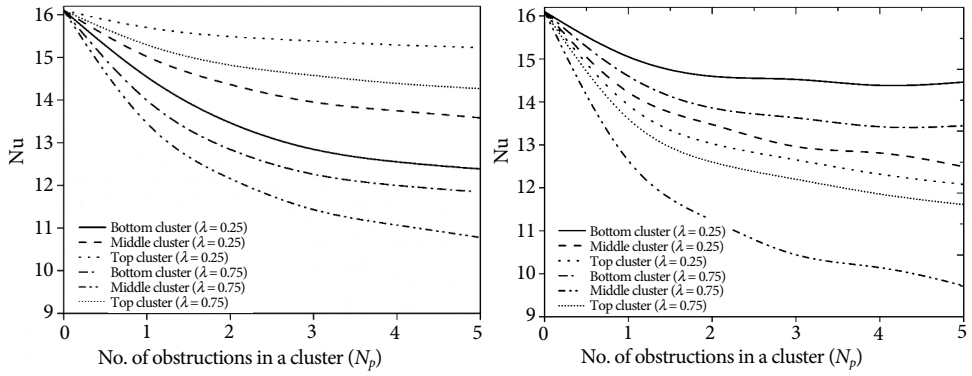

(a) Clustering of obstructions on hot wall (b) Clustering of obstructions on cold wall

Fig. 12. Variation of average Nusselt number for various types of clustered obstructions with respect to number of obstructions in a cluster ($Ra^* = 1000$; $\lambda = 0.25$ and 0.75)

Fig. 13 demonstrates the variation of average Nusselt number with respect to the length of obstructions in a cluster with $N_p = 2$ and 4. There is continuous drop in Nu with increasing values of λ. There is rapid drop in values of Nu for $\lambda \leqslant 0.2$. After that, the drop is very gradual, except for middle clustering where the values of Nu keeps on dropping drastically.

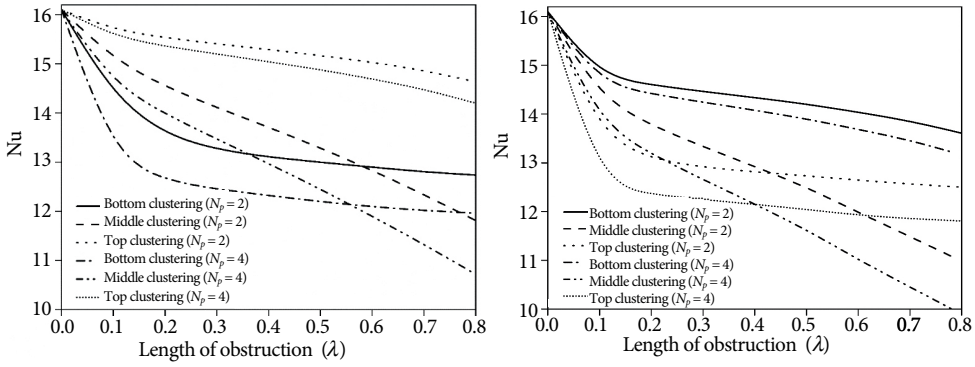

(a) Clustering of obstructions on hot wall (b) Clustering of obstructions on cold wall

Fig. 13. Variation of average Nusselt number for various types of clustered obstructions with respect to length of obstructions in a cluster ($Ra^* = 1000$; $N_p = 2$ and 4)

For clustering on hot wall, maximum reduction is obtained for bottom clustering up to $\lambda \sim 0.5$; while for clustering on cold wall, maximum reduction is obtained for top clustering up to $\lambda \sim 0.4$. After this range, maximum reduction is obtained by middle clustering. This is because, when the length of obstructions is short, the bottom and top-clustered obstructions for hot wall attached and cold wall attached clustering serves as a best obstructer for fluid flow in the high temperature

gradient areas, respectively. However, as the length increases, the bottom clustered obstructions pre-heats the fluid approaching it from a faraway distance causing it to rise immediately after it hits the bottom near the cold wall in a typical convection current. In addition, for longer lengths of middle clustered obstructions, the entire enclosure starts to bifurcate into two rectangular enclosure causing a formation of separate convection current in the top and bottom part of enclosure. Hence, for longer lengths, middle clustered partitions yields the maximum reduction in Nu values.

4.6. Alternate positioning of obstructions

The positioning of obstructions so far was either on hot wall or on cold wall. It is seen that attaching obstructions on cold wall gives slightly greater reduction in Nu. One way as a compromise between the two circumstances, is alternate positioning of obstructions on hot wall and cold wall simultaneously. To evaluate such a model, four types of alternate positioning of obstruction are considered, namely,

1. Type 2H-1C (Two obstructions on hot wall and one on cold wall),
2. Type 1H-2C (One obstructions on hot wall and two on cold wall),
3. Type 3H-2C (Three obstructions on hot wall and two on cold wall),
4. Type 2H-3C (Two obstructions on hot wall and three on cold wall).

Fig. 14 illustrates the streamlines and isotherms developed within a porous enclosure having the above-mentioned four types of alternately positioned obstructions. The length of partitions has been fixed to $\lambda = 0.6$. Irrespective of the total number of partitions, the reduction in value of Nu is larger when the number of obstructions on cold wall is greater than the number of obstructions on hot wall. In previous cases, it was seen that the inner stagnant portion of streamlines was only shortened; whereas, in this case it has not only shortened by a great degree but also is divided into a number of smaller stagnant portions with its magnitude decreasing from top to bottom of the enclosure. This is because the hotter fluid, which is present in the top portion of enclosure, always has greater tendency to move. Almost complete area of enclosure is utilized for deviating the fluid flow using alternate positioning of obstructions. The reduction in the Nu values is about 42% and 65% for the total number of obstructions of 3 and 5, respectively. This can be attributed to the fact that isotherms near the lower half of hot wall and upper half of cold wall have greatly been dispersed and the gradient of temperature has decreased considerably as compared to previous cases.

Fig. 15 illustrates the variation of local Nusselt number along the height of enclosure having the above-mentioned alternated positioning of obstructions with $\lambda = 0.6$ and $\mathrm{Ra}^* = 1000$. It can be clearly seen that, there is a sudden rise in the value of local Nu where obstructions are encountered by the fluid. The rise is significantly higher for obstructions near the lower half of hot wall and upper half of cold wall. The rise in the values indicate the there is sudden rise in temperature

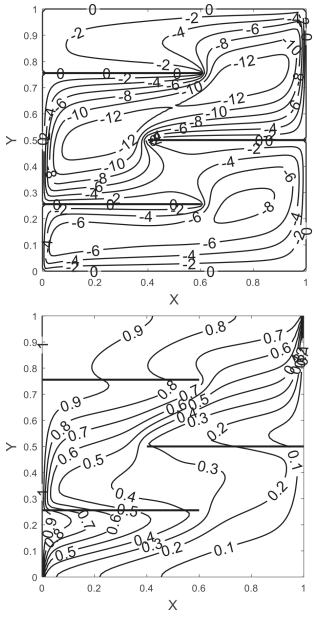

$|\psi|_{\max}$ = 13.25; Nu = 9.31
(a) Type 2H-1C

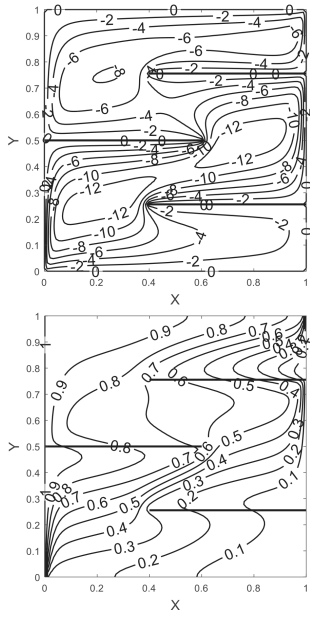

$|\psi|_{\max}$ = 13.19; Nu = 8.96
(b) Type 1H-2C

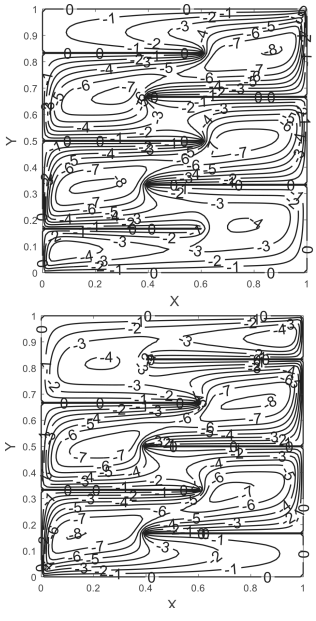

$|\psi|_{\max}$ = 8.22; Nu = 5.51
(a) Type 3H-2C

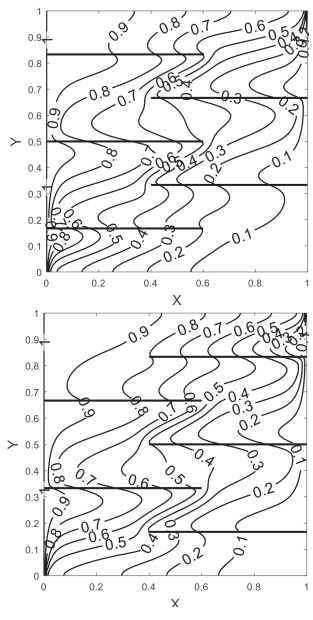

$|\psi|_{\max}$ = 8.12; Nu = 5.38
(b) Type 2H-3C

Fig. 14. Streamlines (up) and isotherms (down) in a porous enclosure having alternately positioned equispaced obstructions ($Ra^* = 1000$, $\lambda = 0.6$).

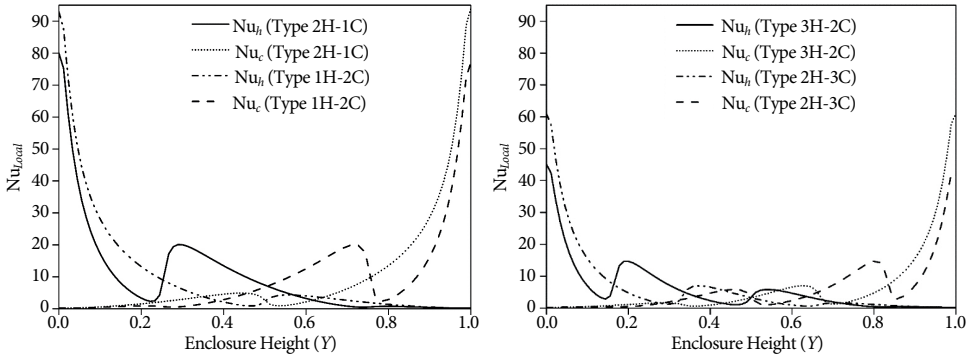

(a) Total number of obstructions – 3 (b) Total number of obstructions – 5

Fig. 15. Variation of local Nusselt number with enclosure height for alternately positioned obstructions having total number of obstructions: (a) $N_p = 3$; (b) $N_p = 5$ ($\mathrm{Ra}^* = 1000$; $\lambda = 0.6$)

gradient in these areas. This can be attributed to the fact, that in the immediate upper part of obstruction, cold fluid tends to move while in the immediate lower part of obstruction, hot fluid moves which is on account of the nature of convection current. Hence, there is larger temperature difference across the obstruction and consequently higher temperature gradient and finally, larger value of local Nu.

5. Conclusions

In the present numerical study, the fluid flow and heat transfer effects of orientation, size, position and combination of multiple internal diathermal obstructions in a fluid-saturated square porous enclosure have been analysed in detail for the following parameters: Number of obstructions (N_p), length of obstructions (λ), modified Rayleigh number (Ra^*), orientation, clustering and alternate positioning. The following conclusions may be drawn from the analysis:

1. The value of average Nusselt number keeps on decreasing as both, the number of obstructions as well as the length of obstructions increases, irrespective of the orientation and positioning of the obstructions.
2. The relation of Nu with N_p is mostly linear for lower value of λ. This relation becomes increasingly quadratic as the value of N_p approaches 0.5 and further. The drop in Nu values is substantial for $N_p \leqslant 5$ after which, the drop is not very significant.
3. Similarly, the relation of Nu with λ is also typically linear for lower value of N_p. This relation becomes progressively quadratic as the value of N_p approaches 5 and further. The reduction in Nu is considerable for $\lambda \leqslant 0.5$. For values of $\lambda > 0.5$, the drop in Nu values is not very significant. The overall reduction in average Nusselt number is slightly greater with obstructions attached explicitly to cold wall irrespective of the values of λ and N_p.

4. Any type of orientation that has obstructions of longer length on lower half of hot wall and/or on upper half of cold wall yields high reduction in Nu of about 65% to 70% for $N_p = 5$ and $\lambda_{\max} = 0.5$.
5. For obstructions attached to hot wall and cold wall, middle clustering yields the maximum reduction in Nu for irrespective of the value of N_p. However, when $\lambda <\sim 0.5$, the maximum reduction for obstructions attached to hot wall and cold wall is obtained for bottom clustering and top clustering, respectively.
6. Alternately positioned obstructions with a greater number of obstructions attached on cold wall than on hot wall yield maximum reduction in Nu.

Manuscript received by Editorial Board, June 25, 2018;
final version, September 10, 2018.

References

[1] D.A.S. Rees. Nonlinear convection in a partitioned porous layer. *Fluids*, 1(3):24, 2016. doi: 10.3390/fluids1030024.

[2] D.A.S. Rees, A.P. Bassom, and G. Genç. Weakly nonlinear convection in a porous layer with multiple horizontal partitions. *Transport in Porous Media*, 103(3):437–448, 2014. doi: 10.1007/s11242-014-0310-y.

[3] Z. M. Al-Makhyoul. Study the effect of non-Darcy flow on natural convection inside rectangular cavity filled with saturated porous medium heated from below using two adiabatic partitions. *Al-Qadisiyah Journal for Engineering Sciences*, 2(2):50–69, 2017.

[4] S.H. Tasnim, S. Mahmud, and A. Dutta. Energy streamlines analyses on natural convection within porous square enclosure with internal obstructions. *Journal of Thermal Science and Engineering Applications*, 5(3):031008, 2013. doi: 10.1115/1.4023603.

[5] M. Sathiyamoorthy and S. Narasimman. Control of flow and heat transfer in a porous enclosure due to an adiabatic thin fin on the hot wall. *Transport in Porous Media*, 89(3):421, 2011. doi: 10.1007/s11242-011-9778-x.

[6] Y. Varol, H.F. Oztop, and I. Pop. Natural convection in a diagonally divided square cavity filled with a porous medium. *International Journal of Thermal Sciences*, 48(7):1405–1415, 2009. doi: 10.1016/j.ijthermalsci.2008.12.015.

[7] Y. Varol and H.F. Oztop. Control of buoyancy-induced temperature and flow fields with an embedded adiabatic thin plate in porous triangular cavities. *Applied Thermal Engineering*, 29(2–3):558–566, 2009. doi: 10.1016/j.applthermaleng.2008.03.018.

[8] Y. Varol, H.F. Oztop, and A. Varol. Effects of thin fin on natural convection in porous triangular enclosures. *International Journal of Thermal Sciences*, 46(10):1033–1045, 2007. doi: 10.1016/j.ijthermalsci.2006.11.001.

[9] S.W. Hsiao and C.K. Chen. Natural convection heat transfer from a corrugated plate embedded in an enclosed porous medium. *Numerical Heat Transfer, Part A: Applications*, 25(3):331–345, 1994. doi: 10.1080/10407789408955952.

[10] P. Vasseur and C.H. Wang. Natural convection heat transfer in a porous layer with multiple partitions. *Chemical Engineering Communications*, 114(1):145–167, 1992. doi: 10.1080/00986449208936020.

[11] A. Bejan and R. Anderson. Heat transfer across a vertical impermeable partition imbedded porous medium. *International Journal of Heat and Mass Transfer*, 24(7):1237–1245, 1981.

[12] Sangita, M.K. Sinha, and R.V. Sharma. Natural convection in a spherical porous annulus: The Brinkman extended Darcy flow model. *Transport in Porous Media*, 100(2):321–335, 2013. doi: 10.1007/s11242-013-0218-y.

[13] Sangita, M.K. Sinha, and R. V. Sharma. Numerical study of natural convection in a spherical porous annulus. *Journal of Porous Media*, 19(3):277–286, 2016. doi: 10.1615/JPorMedia.v19.i3.70.

[14] A.K. Mishra, S. Kumar, and R.V. Sharma. Non-Darcy effects on three-dimensional natural convection in a rectangular box containing a heat-generating porous medium. *Journal of Porous Media*, 19(12):1033–1043, 2016. doi: 0.1615/JPorMedia.v19.i12.20.

[15] K.L. Walker and G.M. Homsy. Convection in a porous cavity. *Journal of Fluid Mechanics*, 87(3):449–474, 1978. doi: 10.1017/S0022112078001718.

[16] A. Bejan. On the boundary layer regime in a vertical enclosure filled with a porous medium. *Letters in Heat and Mass Transfer*, 6:93–102, 1979.

[17] C. Beckermann, R. Viskanta, and S. Ramadhyani. A numerical study of non-Darcian natural convection in a vertical enclosure filled with a porous medium. *Numerical Heat Transfer*, 10(6):557–570, 1986. doi: 10.1080/10407788608913535.

[18] R.J. Gross, M.R. Bear, and C.E. Hickox. The application of flux-corrected transport (FCT) to high Rayleigh number natural convection in a porous medium. In: *Proceedings of 8th International Heat Transfer Conference*, San Francisco, CA, USA,1986.

[19] D.M. Manole and J.L. Lage. Numerical benchmark results for natural convection in a porous medium cavity. In: *Heat and Mass Transfer in Porous Media, ASME Conference* 1992, volume 216, pages 55–60, 1992.

[20] S.L. Moya, E. Ramos, and M. Sen. Numerical study of natural convection in a tilted rectangular porous material. *International Journal of Heat and Mass Transfer*, 30(4):741–756, 1987. doi: 10.1016/0017-9310(87)90204-3.

[21] A.C. Baytas and I. Pop. Free convection in oblique enclosures filled with a porous medium. *International Journal of Heat and Mass Transfer*, 42(6):1047–1057, 1999. doi: 10.1016/S0017-9310(98)00208-7.

[22] O.V. Trevisan and A. Bejan. Natural convection with combined heat and mass transfer buoyancy effects in a porous medium. *International Journal of Heat and Mass Ttransfer*, 28(8):1597–1611, 1985. doi: 10.1016/0017-9310(85)90261-3.